

Received 00th
January 20xx,
Accepted 00th
January 20xx

DOI:
10.1039/x0xx00
000x

www.rsc.org/

Organic Energy Devices from Ionic Liquids and Conducting Polymers

Robert Brooke,^{a,b} Manrico Fabretto,^b Marta Krasowska,^b Pejman Talemi,^{b,c} Samuel Pering,^d Peter J Murphy,^b Drew Evans^{b*}

Supplementary Information

Materials and Methods:

Materials. The ionic liquids, 1-ethyl-3-methylimidazolium bis(trifluoromethylsulfonyl)imide (EMIM-TFSI), 1-butyl-3-methylimidazolium bis(trifluoromethylsulfonyl)imide (BMIM-TFSI), 1-octyl-3-methylimidazolium bis(trifluoromethylsulfonyl)imide (OMIM-TFSI), 1-decyl-3-methylimidazolium bis(trifluoromethylsulfonyl)imide (DMIM-TFSI), 1-dodecyl-3-methylimidazolium bis(trifluoromethylsulfonyl)imide (DDMIM-TFSI), tributylethyl-phosphonium diethyl phosphate (TBEP-DEP), tributyl(tetradecyl)phosphonium dodecylbenzenesulfonate (TBTDP-DDBS), ethylammonium nitrate (EAN), 1-butyl-3-methylimidazolium tetrafluoroborate (BMIM-BF₄), trihexyl(tetradecyl) phosphonium bis(2,4,4-trimethylpentyl)phosphinate (THTDPh-BisPhos) and trihexyl(tetradecyl) phosphonium chloride (THTDPh-Cl) were purchased from Iolitec and were of at least 98% purity. 3,4-ethylenedioxythiophene (EDOT, Clevis V2) and iron tosylate (Fe(Tos)₃, Clevis CB-40 V2) were purchased from Heraeus. Poly(ethylene glycol)-poly(propylene glycol)-poly(ethylene glycol) (PEG-PPG-PEG, Pluronic P-123), Mw = 5800 g.mol and lithium perchlorate was obtained from Aldrich. The ionic liquids were purified before use. All other chemicals were used as received.

Poly(3,4-ethylenedioxythiophene) (PEDOT) fabrication

High conductive PEDOT was synthesized using Vapour Phase Polymerization (VPP), similar to previous reports¹, where the oxidant solution, composed of Fe(Tos)₃ (12.3 wt%) and PEG-PPG-PEG (23.1 wt%) in ethanol, was spin coated at 1500 rpm for 25 seconds onto glass or indium tin oxide (ITO) coated glass substrates. The oxidant coated substrates were placed on a hotplate set at 70 °C for 30 seconds to evaporate the solvent. The substrates were then

^a Linköping University, Department of Science and Technology, Organic Electronics, SE-601 74 Norrköping, Sweden

^b Future Industries Institute, University of South Australia, Mawson Lakes, South Australia, 5095 Australia

^c School of Chemical Engineering, University of Adelaide, Adelaide, South Australia, 5001 Australia

^d Department of Chemistry, University of Bath, Bath, BA2 7AY, United Kingdom

immediately placed into the VPP chamber and removed after 25 minutes. The chamber was operated at 45 mbar at 35 °C with the monomer independently heated to 45 °C. The

inherently conducting polymer (ICP) thin films were annealed on a hotplate set at 70 °C for 2 minutes followed by ethanol washing.

Poly(Pyrrole) (PPy) and Poly(thiophene) (PTh) fabrication

Both PPy and PTh were synthesized using the outlined above for PEDOT, which the following variations. Firstly, the EDOT monomer was exchanged for either pyrrole or thiophene respectively. Secondly, the operating pressure of the VPP chamber was standard atmospheric pressure. The polymerization time was extended to 1 hour. The subsequent annealing and washing steps were are per the PEDOT process.

Abbreviated Name	Anion Structure	Cation Structure	Interaction with PEDOT
EMIM-TFSI			
BMIM-TFSI			
OMIM-TFSI			
DMIM-TFSI			
DDMIM-TFSI			

Table S1: Typical IL composed of hard acid cations with the same soft base anion and their interaction with highly conductive PEDOT

Ionic liquid purification, water content determination and interactions with PEDOT

Water, halide ions and organic residues in ILs are known to influence properties such as viscosity, density and the structure at the interface^{2,3}. To reduce the water content and volatile

compounds to negligible values, a moderate vacuum (0.1 Pa) at moderate temperature (70°C) was applied for 48 h to all ILs. The water content in the ILs was determined using a Metrohm 899 Karl Fischer coulometer. The analyte used for the coulometric Karl Fischer titration was HYDRANAL-Coulomat AG (Sigma Aldrich). Water content for the ILs were as follow: EAN – 540 ppm; BMIM-BF₄ – 320 ppm; EMIM-TFSI, BMIM-TFSI, OMIM-TFSI, TBEP-DEP, TBTDP-DDBS, and THTDPh-Cl - below 200 ppm, DMIM-TFSI, DDMIM-TFSI, and THTDPh-BisPhos below 100 ppm.

An investigation into different cations, or more specifically the carbon chain on the imidazole molecule, was performed to observe the effect (if any) the change has on the ICP.

Atomic Force Microscopy (AFM) experiments

Swelling Observations (no external applied voltage)

The thickness and morphology of PEDOT surfaces in air and in ILs were characterised using Atomic Force Microscopy (AFM). MultiMode® 8 instrument (Bruker, USA) with Nanoscope V controller (Bruker, USA) was used to perform imaging in tapping (intermittent contact) and ScanAsyst modes in air and liquid environment. The AFM base was placed on an active antivibration table (Vision IsoStation, Newport), and equipped with a vertical engagement scanner “J” (maximum scan range 125 µm in x and y directions, and nominal 5 µm in z direction). For tapping mode in air rectangular cantilevers of resonance frequency between 140 and 390 kHz, spring constant between 3.1 and 37.6 N/m, and silicon tip of the radius of curvature of 10 nm (NSG10, NT MDT) were used. For Scan Asyst in air silicon nitride triangular probes of resonance frequency between 70 and 95 kHz, spring constant between 0.4 and 0.8 N/m, and silicon nitride tip of the nominal radius of 2 nm (ScanAsyst AIR, Bruker) were used. For imaging in ILs either triangular silicon nitride triangular probes of nominal resonance frequency between 56 and 75 kHz, spring constant between 0.24 and 0.48 N/m, and silicon nitride tip of the nominal radius of 10 nm (DNP, Bruker) or triangular silicon nitride triangular probes of nominal resonance frequency between 150 and 200 kHz, spring constant between 0.7 and 1.4 N/m, and silicon nitride tip of the nominal radius of 10 nm (ScanAsyst FLUID, Bruker) for image acquisition in tapping and ScanAsyst mode, respectively.

To avoid thermal drift the AFM was left to equilibrate with the laser switched on for about 30 minutes prior the first AFM image was recorded. To eliminate possible artefacts originating from the feedback control ‘trace’ and ‘retrace’ signals were recorded at very slow scan rate (0.99 Hz and below in air, and 0.25 Hz and below in ILs).

All AFM experiments were conducted inside a clean room (Class 1000) at a temperature of 22 ± 1 °C and relative humidity of 39 ± 2%. The images were processed using WSxM 5.0 Develop 6.5.⁵

PEDOT-Tos was deposited on cover-glass disks with a diameter of 15 mm which were scored through the centre. The thickness and morphology of the PEDOT films in air were

obtained by imaging across the scratch made in the PEDOT film. For comparative purposes, images of the ICP in air were used as the control thickness. Note that several different samples of PEDOT were prepared and their thicknesses are different.

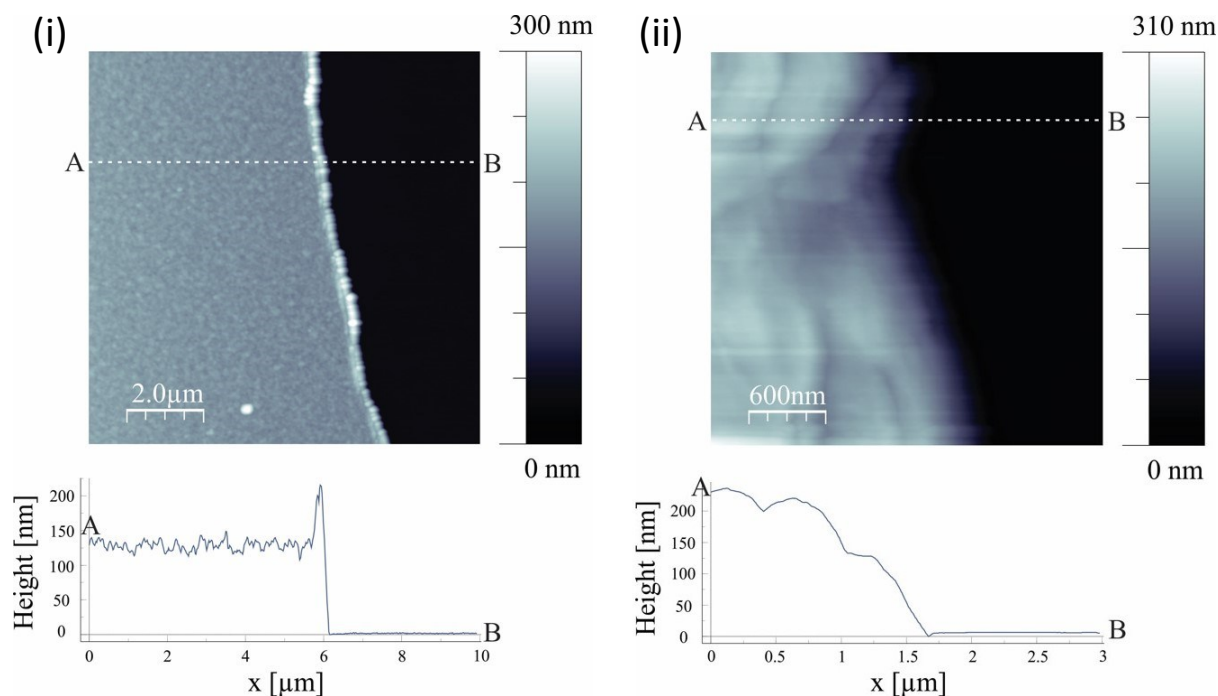


Figure S1: (i) Top: 5 x 5 μm AFM height image of PEDOT in air after the sample has been scored. Bottom: cross section (along the A-B dashed line) shows thickness at various points.

(ii) Top: 3 x 3 μm AFM height image of PEDOT in BMIM-TFSI. Bottom: cross section (along the A-B dashed line) shows thickness at various points.

The thickness of the PEDOT film in air in Figure S1i is an average of 135 nm as shown by the cross sections. Scoring the PEDOT film may lead to (partial) lifting of the edge of PEDOT film. This can be seen in Figure S1i - the edge of PEDOT film appears brighter (thus higher) and the cross section at the edge is higher than the thickness of the film. Whenever possible this effect was avoided, however in some cases the PEDOT film had the lifted edge along entire scratch. In such situations the height of the edge was disregarded when thickness measurements were taken.

Once the PEDOT film thickness was determined¹ from the image the tip was removed and a tip designed for imaging in fluids was inserted. After injecting IL and letting the laser to equilibrate the imaging of the scratch, at very low scan speeds (0.25 Hz and below, depending on the IL viscosity) was performed.

The AFM image and cross sections in Figure S1ii show the PEDOT film has swollen. The sharp features present when PEDOT is imaged in air have been replaced with rounded, bulky

features. The average thickness taken from the above image is 190 nm which is 55 nm more than PEDOT in air (a 34 % increase). While difficult to observe in the thickness images, the morphology of the PEDOT film has been altered by the IL. The sharpness of the PEDOT film in Figure S2 is lost when the ionic liquid is introduced. For further investigation, smaller scan sizes were employed to illuminate the differences between PEDOT in air and PEDOT in BMIM-TFSI.

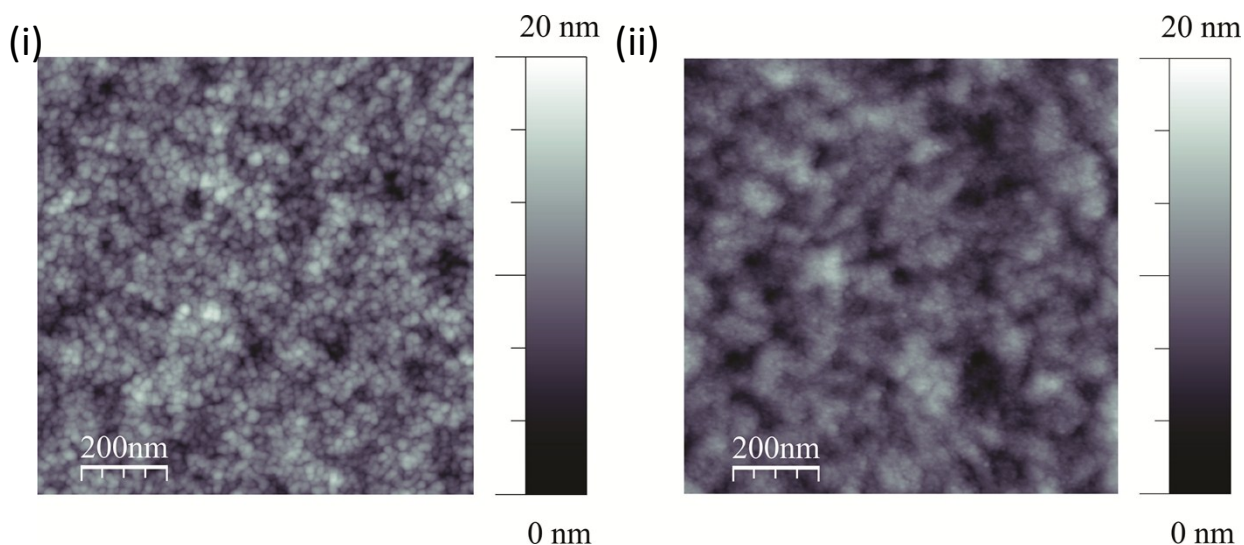


Figure S2: Morphological AFM images of (i) PEDOT in air and (ii) PEDOT in ionic liquid (BMIM-TFSI)

The morphological comparison of PEDOT in air and in BMIM-TFSI in Figure S2 shows two very different morphologies. It can be clearly seen that the PEDOT in IL has larger features while the grain size in the PEDOT in air sample are relatively small. It is assumed there is enough interaction with the IL to cause a change in the morphology and swelling of the ICP. Note that this swelling has occurred for an IL that was not observed to reduce the PEDOT (Table S1).

The same procedure was used to observe the swelling of PEDOT in BMIM-BF₄. That is, the scored PEDOT was imaged in air before being immersed in BMIM-BF₄ followed by further thickness measurements. It is expected that due to the increased viscosity of the BMIM-BF₄ that the AFM images will be of a lesser quality.

¹ In order to avoid any artefacts in the PEDOT film thickness resulting from differences between tips used for imaging in air and in ILs we did perform several scans of PEDOT surface in air using AFM tips designated for imaging in fluid. The PEDOT film thickness extracted from such AFM images was the same as the thickness obtained from the AFM images recorded using tip designated for imaging in air.

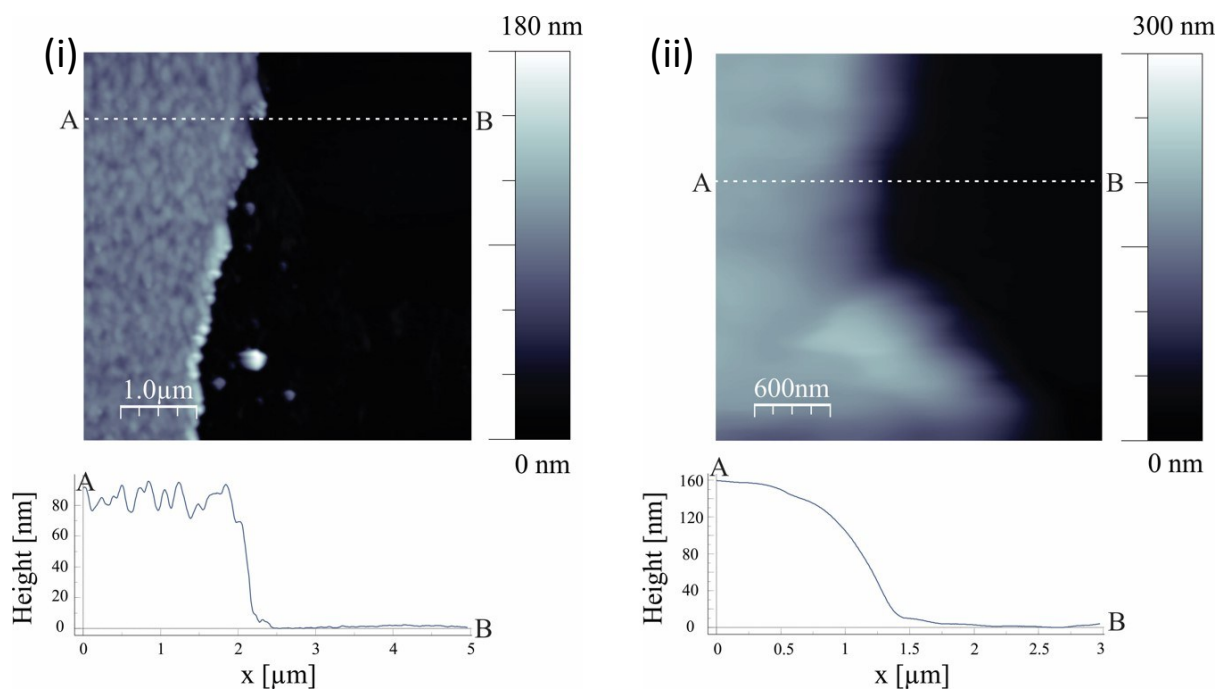


Figure S3: (i) AFM image of PEDOT in air with cross sections for thickness measurements. (ii) AFM image of PEDOT in BMIM-BF₄ with cross sections for thickness measurements

It can be seen from Figure S3ii that the PEDOT film has again lost the sharp peaks that were observed when imaged in air (Figure S3i). Although this suggests the morphology is changing similar to that when PEDOT was immersed in BMIM-TFSI, obtaining high quality images of the morphology was impossible due to the increased viscosity of the BMIM-BF₄. The difference between the PEDOT in air and PEDOT immersed in BMIM-BF₄ was recorded at 65.4 nm or a 55 % increase.

Swelling experiments (external applied voltage)

Carbon tape was employed for electrical connection of the voltage supply to the sample, and created an electrochemical set up with PEDOT acting as the anode and cathode with the IL acting as the electrolyte while conducting AFM (See Figure 2 in the main text). Voltages of positive 0.9 V and negative 0.9 V from an external power supply were employed to electrochemically oxidise and reduce the PEDOT respectively. Thickness measurements via AFM were taken again with the voltages continuously applied to observe the swelling of the PEDOT film under the externally applied bias.

PEDOT in BMIM-TFSI with external potential

Scanning across the score in the PEDOT film yielded thickness measurements, giving information about the swelling which occurs when an external bias is applied. For comparison, neutral PEDOT (no bias) was scanned first which itself is swollen by the addition of the IL (*see previous section*). The tip was then disengaged from the ICP surface,

the potential applied (continuously) and then the tip was re-engaged with the ICP surface. Therefore, the same region is imaged to that of the neutral PEDOT (position is altered due to thermal drift).

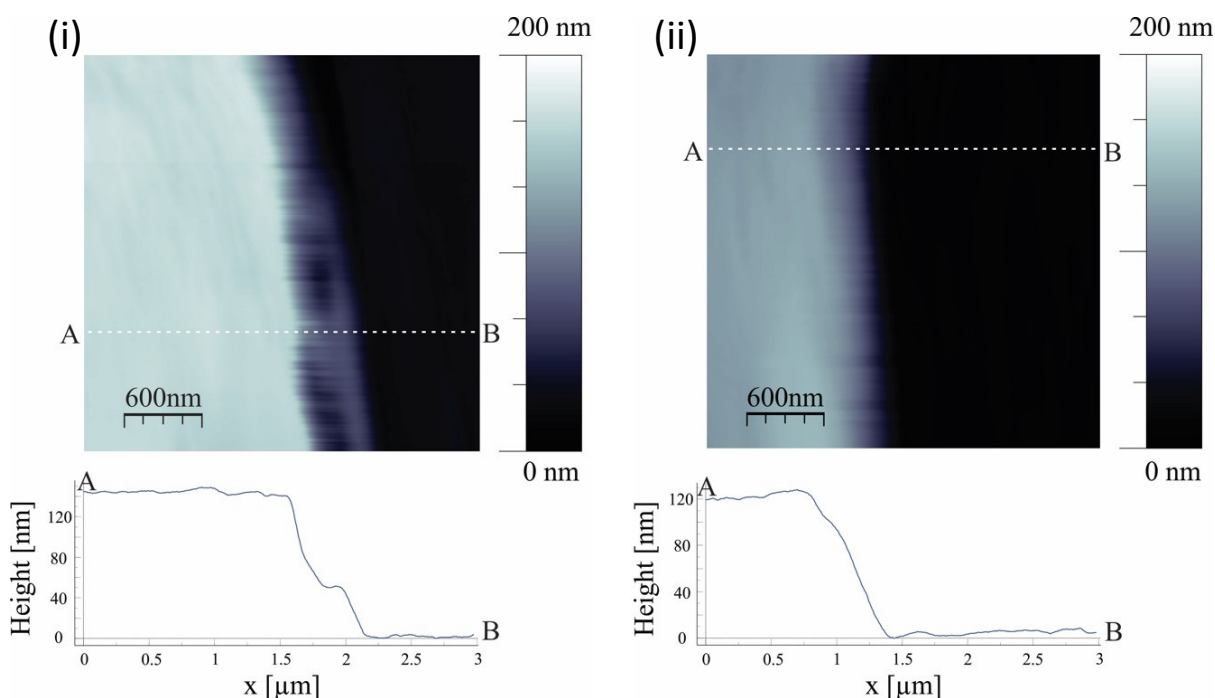


Figure S4: (i) AFM image of PEDOT in BMIM-TFSI under applied voltage of +0.9 V with cross sections. (ii) AFM image of PEDOT in BMIM-TFSI under applied voltage of -0.9 V with cross sections

While the same features (soft edges etc.) can be seen in the positive biased PEDOT film in BMIM-TFSI in Figure S4i, the image is more distorted, thought to be due to the introduction of the applied voltage. The thickness is not thought to be affected since the film is smooth and the scan is clean and straight and therefore any distortion affecting the thickness would be obvious. Figure S4ii shows the image of the PEDOT in BMIM-TFSI with the voltage reversed and a negative potential applied. The same soft edges are observed as seen in the previous images.

Table S2: Average thicknesses given for the PEDOT when no potential, a positive potential (0.9 V) and negative potential (-0.9 V) is applied.

	No Voltage		
	(nm)	Positive (nm)	Negative (nm)
Average Thickness	127	142	121

The thickness measurements in Table S2 provide information about the effect the applied voltages have on the PEDOT film. The thickness for the positive applied voltage (+0.9 V) is higher than that for when no voltage is applied which is itself higher than when a negative voltage (-0.9 V) is applied. This gives an indication of the ingress and egress of the ions composing the IL.

The increase in thickness when a positive bias is applied suggests anions are incorporated into the PEDOT film. This can be rationalized by the positive bias creating more charge defects within the ICP films (more positive charges) that need to be balanced by anions. Therefore the PEDOT film swells more than the neutral PEDOT. The applied negative bias introduces more electrons into the PEDOT film which repel the anions and possibly even the dopant (tosylate anions). Therefore, the PEDOT film under negative bias is not as thick as the neutral or positive biased PEDOT.

PEDOT immersed in BMIM-BF₄ with applied potential

Changing the IL to include a smaller anion such as BF₄⁻ is expected to produce less swelling when the films are experiencing a positive potential. If the theory outlined above is correct, when charge defects are created by the positive potential they will be balanced by the smaller BF₄⁻ anion instead of the larger TFSI⁻ anion. This smaller size therefore should reduce the overall swelling in the PEDOT film. Similar to the PEDOT in BMIM-TFSI experiment, the PEDOT in the neutral state was used as a control before the potentials were applied.

Due to the increased viscosity of the IL the images were taken after an hour of the PEDOT being immersed in the IL, allowing for less disruption during imaging. The same procedure of disengagement, potentially applied (continuously) followed by re-engagement was employed.

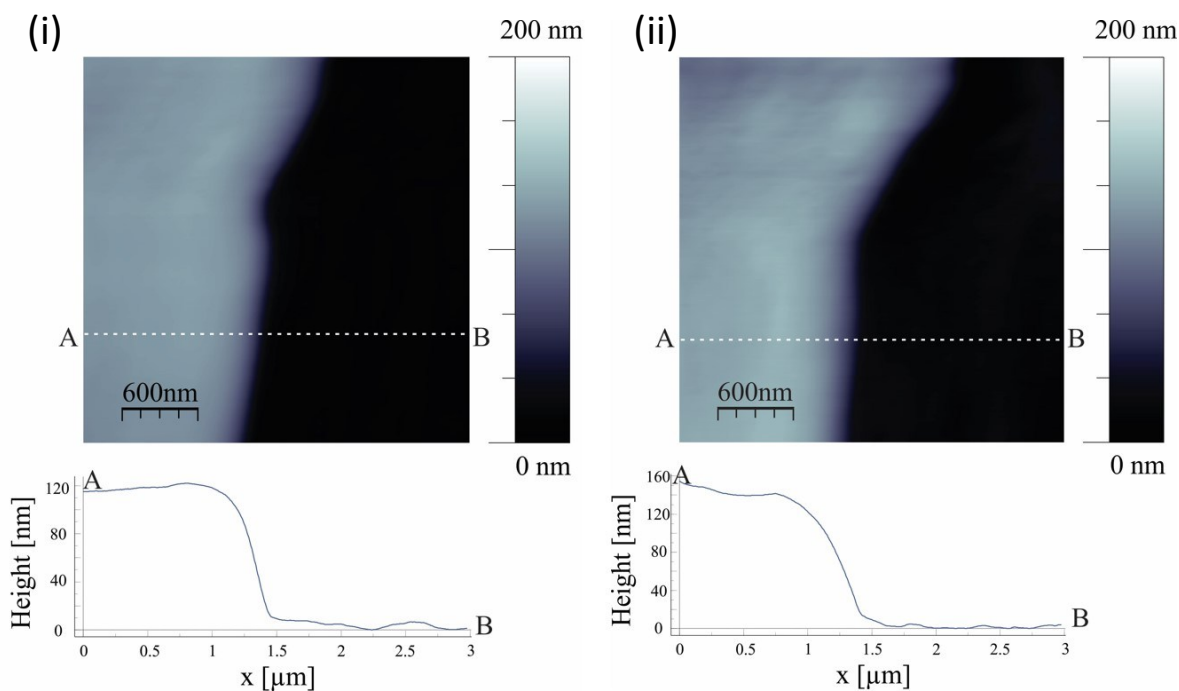


Figure S5: (i) AFM image of PEDOT in BMIM-BF₄ under a positive applied voltage of +0.9 V with cross sections. (ii) AFM image of PEDOT in BMIM-BF₄ under a negative applied voltage of -0.9 V with cross sections.

Figure S5 shows AFM images of PEDOT in BMIM-BF₄ when under positive and negative potential. Many attempts to record the thickness images without the thermal drift were performed but some level of drift was present in every image. This is thought to be due in part to the viscosity as well as the applied voltage.

Table S3: Average thickness values for PEDOT immersed in BMIM-BF₄ with no voltage, positive voltage and negative voltage.

	No Voltage		
	(nm)	Positive (nm)	Negative (nm)
Average			
Thickness	120	119	140

The thickness reported in Table S3 shows the PEDOT thickness under a positive bias is the same when no voltage is applied. While it was expected that the thickness change under this bias would be less dramatic for the smaller anion, it was anticipated that some swelling would be observed. Of perhaps more interest is the increase in thickness of the negatively biased PEDOT compared to the neutral PEDOT. This observation suggests that either the ingress of cations into the PEDOT structure, or the injection of electrons has neutralised charge defects within the PEDOT, thus removing the attractive electrostatic forces that may have been contracting the PEDOT volume.

Comparatively, when THTDPh-BisPhos was placed on a PEDOT thin film it was subsequently reduced and hence could not be switched electrochemically. AFM measurements of PEDOT when immersed in THTDPh-BisPhos with an external applied voltage showed no significant change.

Table S4: Thickness measurements for PEDOT immersed in THTDPh-BisPhos with positive voltage and negative voltage applied.

	Positive	
	(nm)	Negative (nm)
Average		
Thickness	64	66

Table S4 shows the average thicknesses of the PEDOT film when immersed in THTDPh-BisPhos and voltages applied. With no change shown and with both the cation and anion being of relatively large size it is assumed little to no ion movement is occurring. This is rationalized by the PEDOT film being reduced by the IL upon initial intimate contact, and hence no further electrochemical reaction can take place (despite the external bias).

X-ray photoelectron spectroscopy investigation into ion movement

X-ray photoelectron spectroscopy was carried out using (XPS, SPECS, SAGE, Phoibos 150-HAS), fitted with a non-monochromatic Al anode, power 200 W, with a base pressure of 2×10^{-8} mbar. It is believed XPS elemental analysis of ICPs after oxidation and reduction in ILs will shed light on ion ingress and egress. However, studying the change in elemental composition of the ICPs using neat ILs is problematic due to the difficulty in removing the liquid. Therefore, to study the effect sweeping voltages (electrochromic switching) have on the elemental composition of the ICP an ionic solution of LiClO_4 (0.01M) in distilled water was employed. Using this system, the ICPs can be immersed in the ionic solutions, cycled from positive and negative voltages, washed in ethanol, air dried and analysed via XPS. To this end, three initial samples were prepared. The first was soaked in the ionic solution for 20 minutes, the second was oxidised and reduced for 20 cycles and left in its oxidised state and the last underwent the same treatment but left in its reduced state.

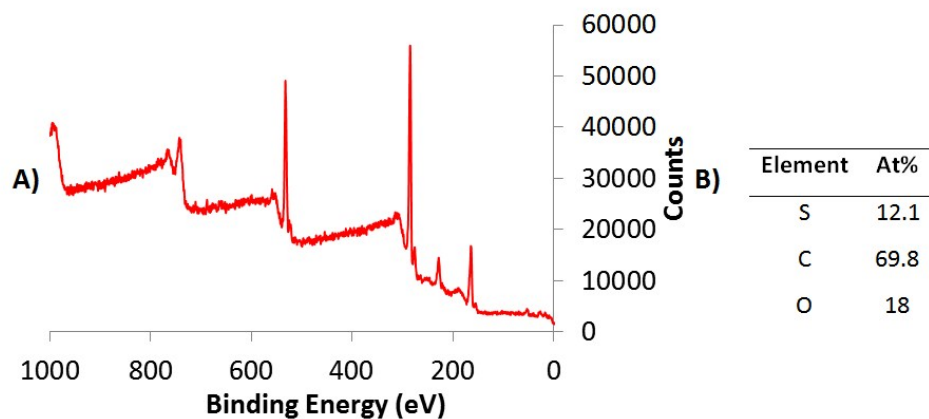


Figure S6: XPS spectra of VPP-PEDOT (via $\text{Fe}(\text{Tos})_3$) before cyclic voltammetry in ionic solution (LiClO_4 in distilled water)

Figure S6 shows the spectra of a PEDOT thin film before the cyclic voltammetry experiment for comparison.

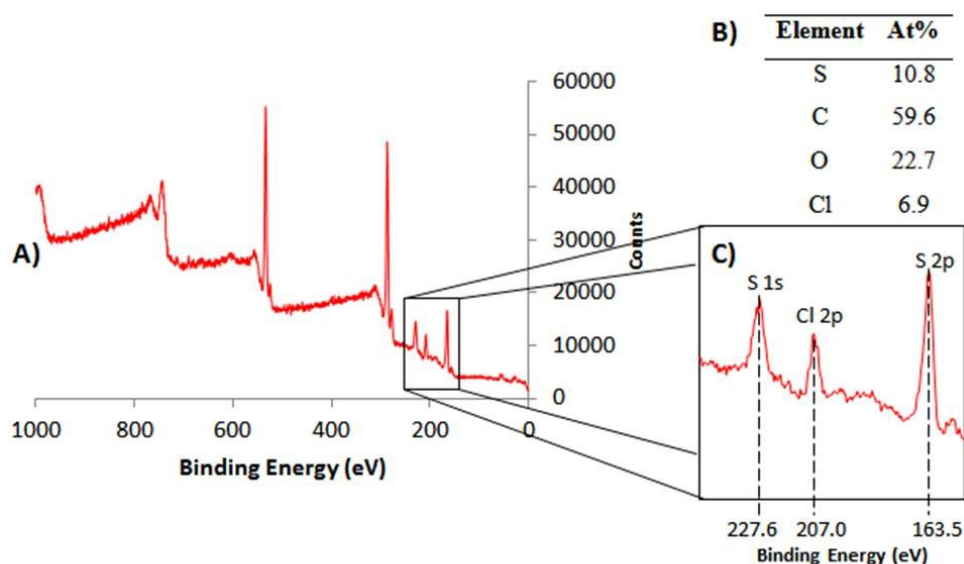


Figure S7: XPS spectra of VPP-PEDOT (via $\text{Fe}(\text{Tos})_3$) after 20 cycles (1.5 V to -1.5 V) in ionic solution (LiClO_4 in distilled water) and kept in the oxidised state

Figure S7 shows the XPS analysis of a PEDOT film after 20 cycles and left in its oxidised state which, by the inset, shows a perchlorate peak at 207 eV of an atomic percentage of 6.9 at%. This result indicates that the anion is introduced and incorporated into the ICP film even after washing with ethanol and air drying.

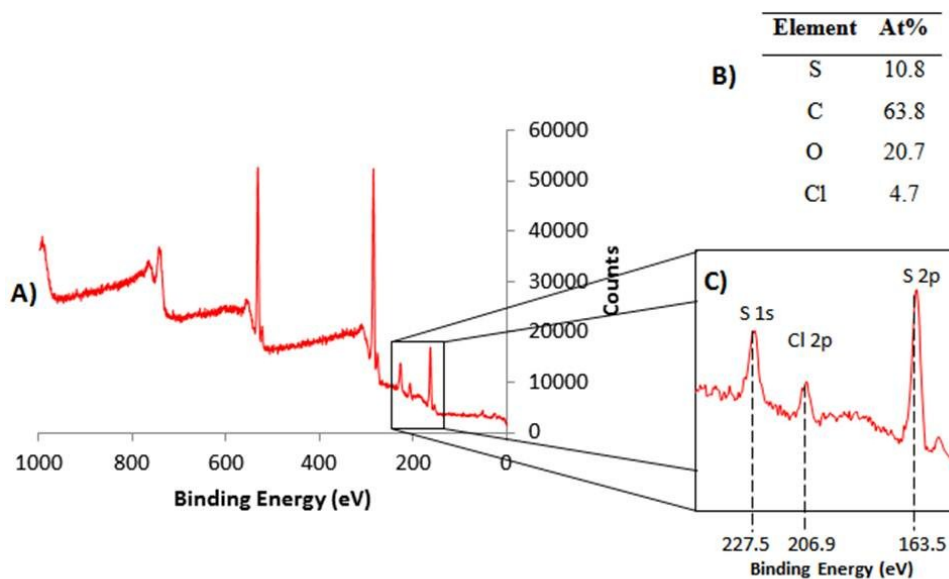


Figure S8: XPS spectra of VPP-PEDOT (via $\text{Fe}(\text{Tos})_3$) after 20 cycles (1.5 V to -1.5 V) in ionic solution (LiClO_4 in distilled water) and kept in the reduced state

Figure S8 shows the XPS spectra of a PEDOT film left in its reduced state after 20 switches and interestingly still shows the perchlorate peak, albeit at a reduced atomic percentage. The perchlorate peak was also shown in the PEDOT sample soaked in the ionic solution without a bias. It is not fully understood why the perchlorate ion is observed for the reduced and soaked sample. One hypothesis is that the ions are trapped within the polymer matrix. Another hypothesis is that the perchlorate ions have replaced the tosylate anions as the dopant. Unfortunately this hypothesis, due to both PEDOT and tosylate containing sulphur, cannot be confirmed or denied using elemental analysis. However, from the XPS spectra, the perchlorate ions are present in higher atomic percentage in the oxidised PEDOT followed by the soaked and lowest for the reduced state (Figure S9) suggesting more perchlorate ions diffuse into the ICP when oxidised. This result correlates well as the oxidised PEDOT should contain more charge defects and need more anions to balance the charge.

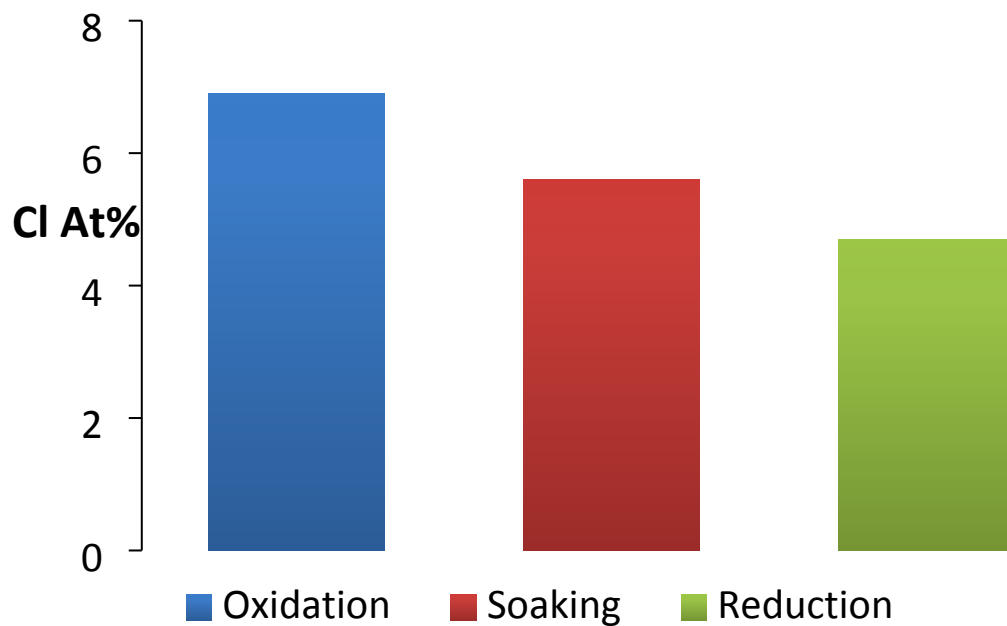


Figure S9: Graph showing the relative perchlorate ions (atomic percent) of PEDOT films in the oxidised, reduced and when soaked.

While the above XPS spectra show the information for the anion within the PEDOT samples, the lithium peak in the spectra is hidden by a cross talk peak between the XPS sources. Therefore, it is not known if LiClO_4 , as a molecule, is trapped within the CP matrix as well as if there is any incorporation of the Li^+ ions when oxidised and reduced. To shed light on these two situations, an Al source was substituted for the Mg source which moves the cross talk peak and allows identification of the lithium peak.

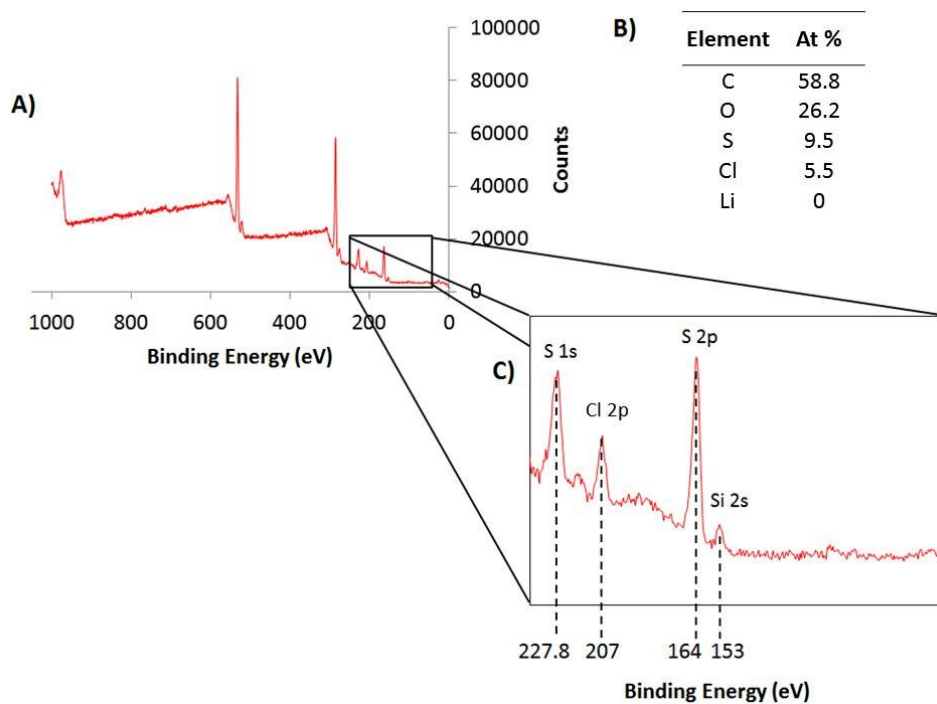


Figure S10: VPP-PEDOT (Tos) left in the reduced state analysed using Al target in the XPS. A) XPS spectra, B) Elemental composition and C) inset of peaks of interest

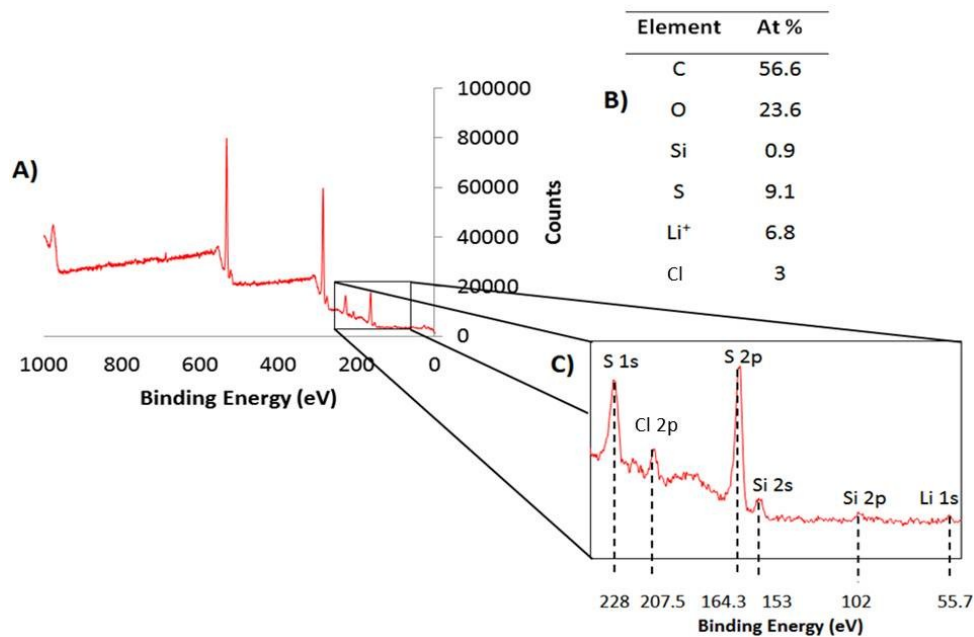


Figure S11: VPP-PEDOT (Tos) left in the oxidised state analysed using Al target in the XPS. A) XPS spectra, B) Elemental composition and C) inset of peaks of interest

The Figures S10 and S11 only show the presence of lithium within the reduced PEDOT film. This result suggests that cations are absorbed into the ICP due to electrons being injected. It is not known how much lithium is present as lithium bound to perchlorate or associated with PEDOT. It is interesting to note that perchlorate was present, but lithium was not, in the PEDOT film soaked (without bias) in the solution. This may be due to the ICP film containing charge defects which attract negatively charged perchlorate ions which displace/replace the tosylate anions (ion exchange).

The trend of the perchlorate atomic percent still remains using the different source as seen in Figure S12. If we assume some of the lithium present in the reduced sample is associated with perchlorate, and not the ICP, the difference between the oxidised and reduced is increased.

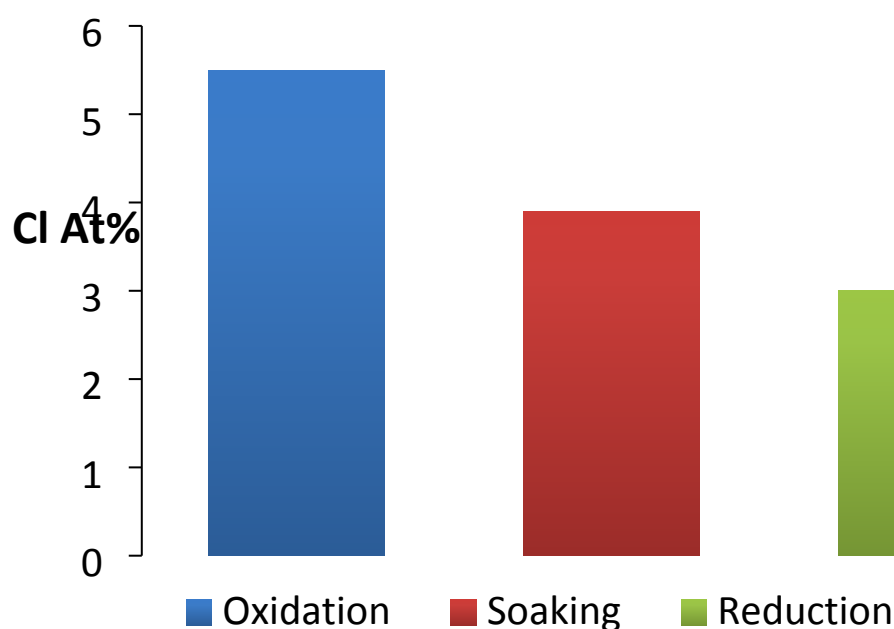


Figure S12: Graph showing perchlorate atomic percentage trend in oxidised, reduced and soaked PEDOT sample using Al XPS source.

Optical Switching investigation

PEDOT films deposited on ITO coated glass substrates were incorporated into a test electrochromic device as seen in Figure S13. The counter electrode was another ITO coated glass substrate and the reference electrode was Ag/AgCl and the device was filled with ionic liquid. A VoltaLab PGZ100 All-in-One device was employed as an external voltage source for electrochromic switching. The voltages used were positive 1.5 V to negative 1.5 V. To record the optical properties and electrochromic behaviour a HunterLab UltraScan Pro spectrophotometer was employed while the voltages were applied.

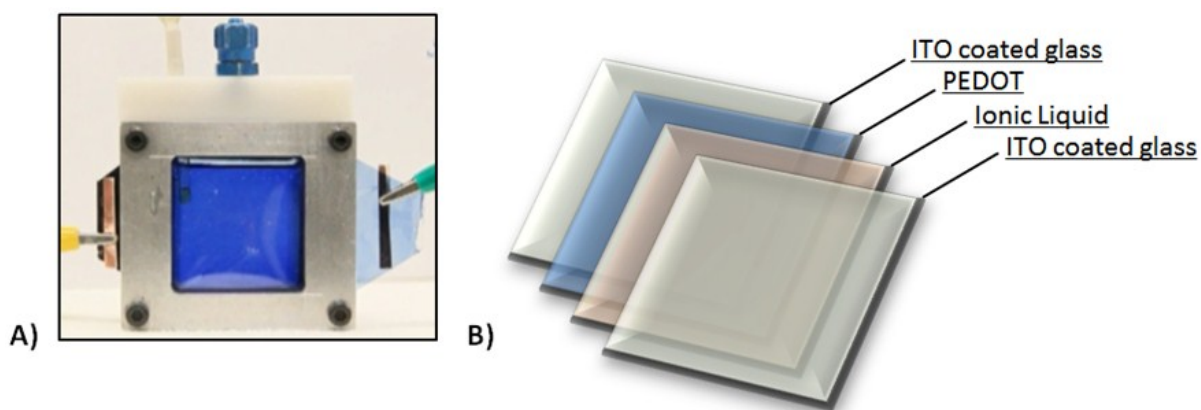


Figure S13: A) image showing the electrochromic test cell B) Schematic showing the layers incorporated in the electrochromic test cell.

Optical Memory investigation

The same test electrochromic device set up for the optical switching investigation was employed for the optical memory investigation. The test electrochromic device was placed in between a photodiode detector and a LED emitting at 560 nm (maximum human photopic response⁶). The device was subject to 0 V to ensure previous voltages applied did not interfere with the experiment. A voltage of negative 1.5 V was then applied to the device for 30 seconds and then disconnected. The relaxation to the neutral state was measured over 30 minutes which was sufficient to observe significant differences between the ILs.

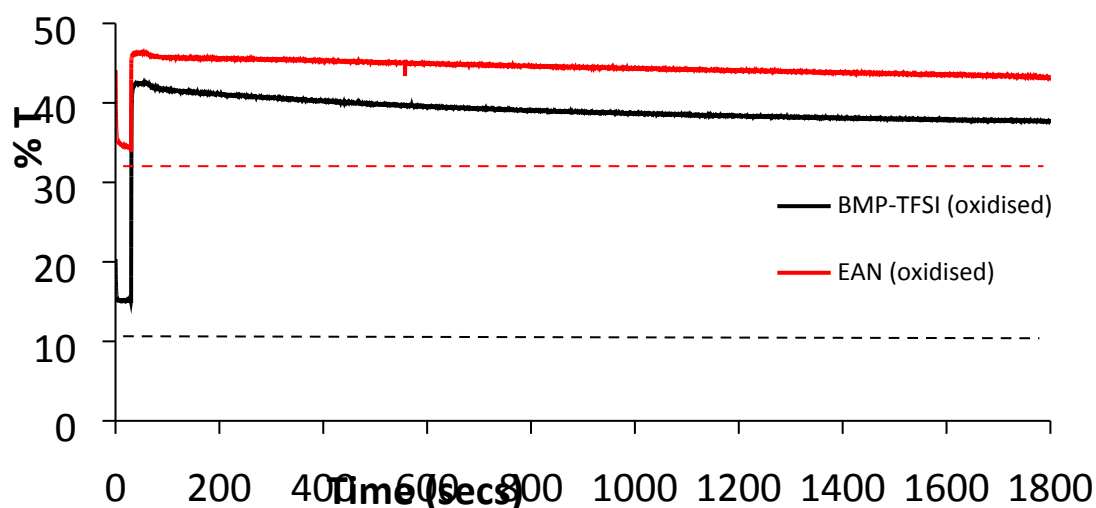


Figure S14: The relaxation of PEDOT-Tos from its oxidized state, back to its neutral state when the system is in open circuit. Dotted lines indicate the PEDOT-Tos in its 0 V neutral state

The optical memory shown in Figure S14 shows the ILs, EAN and BMP-TFSI as they relax from their oxidised states (+1.5 V). It can be seen that the 0 V states of the two are very different with EAN chemically oxidising the highly doped PEDOT. The relaxation curve of the EAN is also less dramatic as the neutral state is closer to the oxidised state when compared to the BMP-TFSI oxidised PEDOT.

Prototype Smart Window

Based on this knowledge, we fabricated a prototype smart window (Fig S15a) in which an IL was encapsulated in a working active OED with PEDOT as the working electrode, and PPy as the counter electrode (both electrodes were deposited onto ITO coated glass substrates). Using the BMP-TFSI IL ensures the absence of any chemical interaction which would otherwise diminish the optical memory of the active OED. Given the counter electrode undergoes the opposing electrochemical reaction to PEDOT, the net result of adding the PPy counter electrode to the smart window is an enhanced darkening when PEDOT reduces (“Dark Mode”) and a yellow hue when the PEDOT oxidises (“Light Mode”) as shown in Fig S15b. The optical memory was measured over a 12 hour period for both the Dark and Light Mode for the smart window device (Fig S15c). From these prototype device experiments, the optical memory is observed to extend over a timeframe of many hours, with 10% relaxation back towards the neutral state of the device occurring at 1.5 and 0.8 h for the Dark and Light Modes respectively. The difference in relaxation rates between the prototype device and the test cell in Figure 3 in the main text is related to differences in electrode spacing as well as the level of device encapsulation. After 12 h, the prototype smart window had relaxed by 50% and 60% for the Dark and Light Modes respectively. In practice, a short voltage pulse of the order of a few μs every hour would be sufficient to maintain the working device in its operational mode (greater than 90% of the Dark or Light Mode), demonstrating the very lower power consumption requirement that can be achieved simply by selecting the correct IL based on the information presented herein.

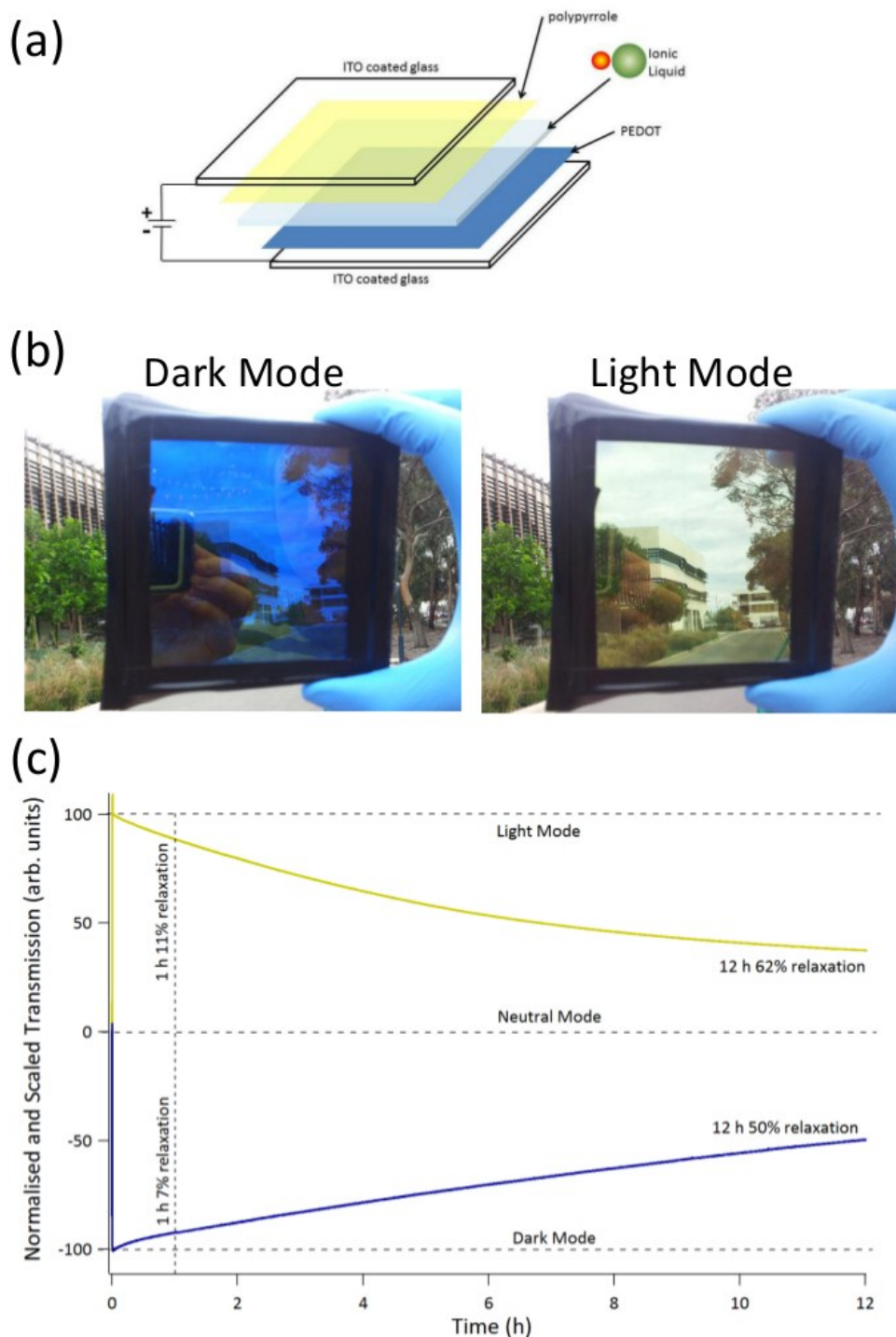


Figure S15. Prototype Smart Window. The optical switching and memory of a prototype smart window is demonstrated, where the device has been designed taking into account the implications of the ICP-IL interactions. (a) The architecture of the device utilises the full encapsulation of BMP-TFSI between a PEDOT working electrode and PPy counter electrode; both deposited on ITO coated glass. (b) The prototype smart window can be switched between its Dark and Light Modes through application of a 1.5 V potential. (c) The relaxation from the Dark and Light Mode of the prototype device occurs over many hours, with the device retaining 50% and 38% of the switched states respectively after 12 hours. A

short voltage pulse of the order of a few μs every hour is sufficient to maintain the device in its fully switched state, demonstrating low power consumption that can be achieved by proper IL selection.

Supercapacitor

Extending knowledge of the ICP-IL interactions to energy storage, a Type I supercapacitor was fabricated using high doped VPP PEDOT-Tos as both electrodes, separated by different ILs. The resultant specific capacitance of the prototype devices was normalised to the peak for the BMP-TFSI IL to give the relative changes in properties of the device. Interestingly, literature suggests that the dielectric constant of these ILs should be similar⁷, and hence only small variation in specific capacitance is anticipated using prior assumptions for no chemical interactions. However, as shown in Fig S16, the specific capacitance can vary greatly depending on the IL chosen, even if their dielectric constant is comparable.

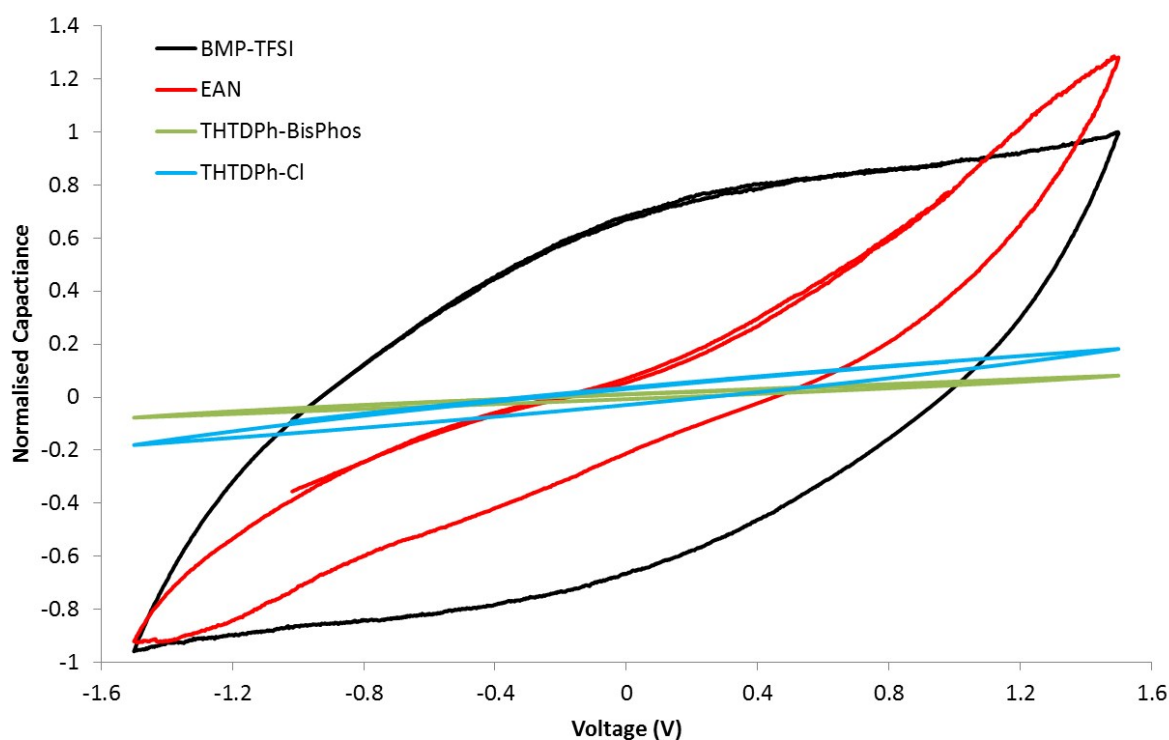


Figure S16: Prototype Type I (symmetric) supercapacitor. The capacitance of each device was normalised to the peak capacitance using the BMP-TFSI IL (black). Note that the EAN (red) achieves comparable peak capacitance, though the energy density is greatly reduced. In the case of the two THTDPh (blue = Cl, green = BisPhos) ILs, there is a five-fold reduction in the specific capacitance of the prototype device.

References

- (1) Fabretto, M. V. *et al. Chem. Mater.* **2012**, 24, 3998.
- (2) Baldelli, S. *J. Phys. Chem. B* **2003**, 107, 6148.
- (3) Seddon, K. R., Stark, A. & Torres, M.-J. *Pure Appl. Chem.* **2000**, 72, 2275.
- (4) Garnier, F., Tourillon, G., Barraud, J. Y. & Dexpert, H. *J. Mater. Sci.* **1985**, 20, 2687.
- (5) Horcas, I. *et al. Rev. Sci. Instr.* **2007**, 78.

- (6) Fabretto, M. *et al. Electrochem. Commun.* **2007**, 9, 2032.
- (7) Choi, U. H. *et al. Macromolecules* **2013**, 46, 1175.